Available online at www.sciencedirect.com

SciVerse ScienceDirect

Geochimica et Cosmochimica Acta 85 (2012) 142–159

Geochimica et Cosmochimica Acta

www.elsevier.com/locate/gca

The Tafassasset primitive achondrite: Insights into initial stages of planetary differentiation

Kathryn G. Gardner-Vandy [a,*], Dante S. Lauretta [a], Richard C. Greenwood [b], Timothy J. McCoy [c], Marvin Killgore [d], Ian A. Franchi [b]

[a] Lunar and Planetary Laboratory, University of Arizona, 1629 E. University Blvd., Tucson, AZ 85721, United States
[b] Planetary and Space Sciences Research Institute, The Open University, Walton Hall, Milton Keynes, MK7 6AA, United Kingdom
[c] Smithsonian Institution, National Museum of Natural History, P.O. Box 37012, MRC 119, Washington, DC 20013, United States
[d] Southwest Meteorite Laboratory, Payson, AZ 85547, United States

Received 11 April 2011; accepted in revised form 8 January 2012; available online 2 February 2012

Abstract

Tafassasset is an exceptional meteorite that has been linked to both the CR chondrites and the primitive achondrites. Because previous evidence suggests it might be a primitive achondrite from a known chondrite type, we have undertaken a study of the petrology, geochemistry, and formation history of the meteorite. Tafassasset is predominantly FeO-rich olivine (~58%) yet contains abundant Fe,Ni-metal (~10 vol.%) and sulfide (~3 vol.%). Other phases include high- and low-Ca pyroxene, plagioclase, chromite, and phosphate. It has a recrystallized texture, containing equigranular grains that often meet at 120° triple junctions. There are no relict chondrules in the thin sections examined, although they have been reported previously. Electron microprobe analyses reveal homogeneous olivine ($Fa_{28.6}$), both low-and high-Ca pyroxene ($Fs_{23.6}Wo_{3.7}$ and $Fs_{12.2}Wo_{39.3\pm1}$), a range of plagioclase composition (An_{23-47}), Fe,Ni-metal (with 5.3–36.6 wt.% Ni and 0.1–0.8 wt.% Co), troilite, chromite, and Ca–phosphate. Bulk composition analyses reveal two chips depleted in refractory lithophile and some siderophile elements compared to CI chondrites. Exceptions are enrichments in Fe, Ni and Co. A third chip is essentially chondritic in bulk composition. Different stones of the meteorite have slightly different oxygen isotope composition, yet all lie in the CR chondrite trend with one in the acapulcoite–lodranite field. Thermodynamic calculations show that Tafassasset equilibrated at a temperature above the Fe,Ni–FeS eutectic and at an oxygen fugacity of ~IW-1. The texture, heterogeneous distribution of mineral phases, plagioclase composition, two-mineral closure temperatures, and bulk composition all provide evidence that Tafassasset partially melted on its parent body. A comparison with the CR chondrites, the brachinites, and two anomalous achondrites indicates that Tafassasset is most similar to ungrouped primitive achondrites Lewis Cliff (LEW) 88763 and Divnoe, and to the brachinites in overall petrography, modal mineralogy, mineral compositions, oxidation state, and bulk composition. The comparison also excludes the possibility that Tafassasset formed by partial melting of a CR chondrite. Tafassasset is a primitive achondrite and likely evolved on a parent body that experienced incomplete melting, never reached isotopic homogeneity, and was from the same oxygen isotopic reservoir as the CR chondrite parent body.

1. INTRODUCTION

Found on February 14, 2000 in the Ténéré desert region of the Sahara in Niger, Tafassasset is an olivine-dominated and metal-rich recrystallized meteorite with an ambiguous classification. It has been linked and compared to two groups of meteorites: the CR chondrites and the primitive achondrites. The only published study of Tafassasset is on the noble gas inventory of the meteorite, and the authors were unable to reach a definitive conclusion on its origin (Patzer et al., 2003). Likewise, it is disadvantageous that the Tafassasset name was given to a group of 26 meteorites (totaling ~ 110 kg) that were found in the same location,

* Corresponding author.
E-mail address: kgardner@lpl.arizona.edu (K.G. Gardner-Vandy).

0016-7037/$ - see front matter © 2012 Elsevier Ltd. All rights reserved.
http://dx.doi.org/10.1016/j.gca.2012.01.014

six of which were collected a year later in March 2001, and there is marked textural heterogeneity between samples (Russell et al., 2002). In addition, J. Otto of the Universität Freiburg reported a 36 kg sample named Te-1 found in March 2000 in the same location as the 26 Tafassasset stones.

The Meteoritical Bulletin reflects two different classifications of Tafassasset (Russell et al., 2002). Tafassasset was first classified by Bourot-Denise et al. (2002) as a metamorphosed CR chondrite based upon: (1) an oxygen isotope composition similar to the CR chondrites, and (2) the presence of mm-sized, metal-bearing relict chondrules similar to the chondrules found in Renazzo. A second study by Zipfel et al. (2002) confirmed a pairing of Tafassasset and Te-1 and found that both have refractory lithophile element compositions depleted relative to the CI chondrites, with Al/Mg and Mn/Mg ratios more like those of other primitive achondrites. They relate the two meteorites' compositions to incipient partial melting and exclude a relationship between the CR chondrites and Tafassasset.

Subsequent studies of Tafassasset elucidate little more in the way of definitive classification and formation history of the Tafassasset meteorite. Patzer et al. (2003) calculated the cosmic ray exposure (CRE) and gas retention ages of Tafassasset and discuss the shielding conditions and trapped noble gas content of the meteorite. They found the CRE age to be 76.1 ± 15.2 Ma, quite different from the CR chondrites' CRE ages of between ~6 and ~9 Ma. They find that Tafassasset's CRE age, low ^{132}Xe concentrations, low ^{36}Ar/^{132}Xe ratio, and the absence of a solar component all discriminate Tafassasset from the CR chondrites. Likewise, they note that the occurrence of radiogenic ^{129}Xe may support a connection between Tafassasset and the brachinites. They give the caveat, however, that these apparent similarities could be explained by the metamorphosed nature of Tafassasset as a more consolidated CR chondrite. They conclude that the noble gas inventory of Tafassasset is inconclusive to its origin and classification.

Nehru et al. (2003) note textural and mineralogical similarities between Tafassasset and Brachina, the type specimen of the brachinite meteorites, and discuss Tafassasset as a metal-rich brachinite-like meteorite similar in oxygen isotopic composition to Lewis Cliff (LEW) 88763, a "brachinite" that Swindle et al. (1998) determined is an ungrouped primitive achondrite. Nehru et al. (2003) conclude that there are two groups of brachinites in existence: one main group and another group that includes LEW 88763 and Tafassasset which may have evolved from a different parent body that was more similar to that of the CR chondrites.

Most recently, Göpel et al. (2009) conducted a U/Pb and Cr isotopic investigation of Tafassasset. They report a Pb/Pb age between 4.555 and 4.564 Ga as well as ^{53}Cr and ^{54}Cr values that agree with Cr isotopic composition reported for Renazzo.

It is clear that further investigation of Tafassasset is needed in order to understand its origin and genetic relationship to other meteorite groups. No matter what origin is applicable to Tafassasset, its existence in the meteorite collection is remarkable, either as a recrystallized and equilibrated CR chondrite or as a metal-rich brachinite-like primitive achondrite. Because previous evidence suggests the exciting possibility Tafassasset might be a primitive achondrite from a known chondrite type, we have undertaken the following study. Here, we report the petrology, bulk chemistry, oxygen isotope composition, and formation conditions of Tafassasset and discuss its relationship with the CR chondrites and the primitive achondrites in an effort to better understand its origin. We also present oxygen isotope analyses of two brachinites, Northwest Africa (NWA) 3151 and Hughes 026, to use in comparison to the oxygen isotope analyses of Tafassasset. Preliminary findings were reported in Gardner et al. (2007), Gardner-Vandy et al. (2008), and Gardner-Vandy et al. (2009).

2. SAMPLES AND ANALYTICAL TECHNIQUES

We obtained several samples of Tafassasset for analysis. Marvin Killgore of the Southwest Meteorite Laboratory in Payson, Arizona supplied two stones of Tafassasset, including four consecutive polished thin sections from one of the stones. These are designated "Tafa-MK." The Museum National d'Histoire Naturelle in Paris, France supplied two stones of Tafassasset, including two non-consecutive polished thin sections and a chip of the first stone and a polished thin section of the second stone. These samples are designated "Tafa-Paris." The two Tafa-MK stones and one Tafa-Paris stone were split with a rock splitter to obtain material for bulk chemistry and oxygen isotope analyses. Table 1 gives an inventory of the samples used in this study, including the area of each thin section analyzed and the masses of the chips used. Even though we did not obtain material of the Tafassasset stone from the Universität Freiburg in Freiburg, Germany (previously called "Te-1"), we designate it as "Tafa-Freiburg" when we refer to it.

Table 1
Inventory of Tafassasset samples used for study.

Type	Label	Area (mm^2)	Analysis type
Thin section	Tafa-MK1	230	EMPA
Thin section	Tafa-MK2	242	EMPA
Thin section	Tafa-MK3	250	EMPA
Thin section	Tafa-MK4	243	EMPA
Thin section	Tafa-Paris3	114	EMPA
Thin section	Tafa-Paris5,2	111	EMPA
Thin section	Tafa-Paris5,4	168	EMPA
		Total: 1358	
		Mass (mg)	
Chip	Tafa-MKa	86.07	ICPMS
Chip	Tafa-MKb	91.40	ICPMS
Chip	Tafa-Paris5	33.99	ICPMS
		Total: 211.5	
Chip	Tafa-MK	130	O Isotopes
Chip	Tafa-Paris5	70	O Isotopes
		Total: 200	

Tafa-MK denotes material from Marvin Killgore's collection. Tafa-Paris denotes material from the Museum National d'Histoire Naturelle in Paris, France.

2.1. Petrographic analysis

We examined the thin sections of Tafassasset under both plane- and cross-polarized light using the Leica DMLP petrographic microscope at the Lunar and Planetary Laboratory (LPL) to characterize the meteorite's mineralogy and texture. We then analyzed the silicate, metal, and sulfide phases of Tafassasset with the Cameca SX50 electron microprobe at the LPL. We obtained X-ray element maps of all thin sections to locate mineral phases and to calculate modal abundances. We used the Cameca SX100 electron microprobe at the LPL to: (1) obtain high resolution X-ray maps of the TafaMK1 thin section to combine in Adobe Photoshop as 3-color maps, and (2) acquire chromite analyses with vanadium concentrations corrected for Ti interferences. We used the Cameca Peaksight software v4.2 for the SX100 that subtracts the TiK_β line from the VK_α line. Matrix corrections were applied during the peak subtraction. The conditions for electron microprobe analysis (EMPA) were: 15 kV, 20 nA and 1 μm beam for olivine and pyroxene (20 s peak time); 15 kV, 8 nA and 10 μm beam for Na and K in plagioclase (10 s peak time); 15 kV, 40 nA and 1 μm beam for metals and sulfides (20 s peak time); 15 kV, 20 nA and 1 μm beam for oxides (20 s peak time); and 15 kV and 40 nA for X-ray element maps. We calibrated with the following standards for silicate and oxide minerals: diopside for Si, Mg, and Ca; fayalite for Fe, albite for Na, anorthite for Al, orthoclase for K, rhodonite for Mn, rutile for Ti, chromite for Cr, apatite for P, Ni-diopside glass for Ni. Detection limits (in wt.%) for silicates are: 0.03 for Si, 0.03 for Mg, 0.02 for Ca, 0.07 for Fe, 0.03 for Na, 0.02 for Al, 0.02 for K, 0.04 for Mn, 0.03 for Ti, 0.05 for Cr, and 0.08 for Ni. Detection limits (in wt.%) for chromite are: 0.02 for Mg, 0.02 for V, 0.02 for Ti, 0.05 for Mn, 0.08 for Cr, 0.08 for Fe, 0.08 for Ni, 0.02 for Al, 0.02 for Si, and 0.01 for Ca. For metal and sulfide analyses, elemental metal standards (Fe, Ni, Co, Cr and Ti) and chalcopyrite (S) were used. Detection limits (in wt.%) for metals and sulfides are: 0.05 for Fe, 0.05 for Ni, 0.05 for Co, 0.02 for S, 0.02 for Cr, 0.01 for Ti, 0.1 for Cu, 0.01 for Si, 0.02 for Al. We use only silicate, metal and sulfide EMPA data with totals between 99% and 101% and oxide data with totals between 98.5% and 101.5%. Element maps were made for Na, Mg, Al, Si, P, S, K, Ca, Ti, Cr, Fe, Co, and Ni. These maps were then used with the program IQmaterials™ by Media Cybernetics to calculate modal abundances in the thin sections.

2.2. Bulk composition analysis

We analyzed three chips of Tafassasset by inductively coupled plasma mass spectrometry (ICP-MS) using the ThermoFinnigan Element2 high resolution single collector magnetic sector ICP-MS at the LPL. Each chip of Tafassasset was dissolved in 2 mL concentrated HNO_3 and 1 mL concentrated HF in Teflon containers on a 120 ± 5 °C hotplate for 10 days. Each sample was placed in an ultrasonic bath for ~10 min. approximately every 24 h. The digested samples were then evaporated on a 100 ± 5 °C hotplate to almost dryness, at which point 5 mL of 5% HNO_3 was added. This solution was diluted with 5% HNO_3 so that final analytical solution for each sample had 100 ppm total dissolved solids.

Our standards were the Geological Society of Japan standard basalt JB-2 and a series of custom-made solutions of primitive achondrite ratios made from High-Purity Standards single-element solutions. We utilized JB-2 strictly as an internal standard, not as a proxy for Tafassasset elemental concentrations. We modeled the custom-made matrix solution after the major element composition of the well-studied primitive achondrite Divnoe using standard solutions of Fe, Mg, Ca, Al, Cr, Mn, Ni and S (Petaev et al., 1994). Successive dilutions of this matrix solution were used to quantify major elements. For trace elements, we employed the standard addition technique, spiking four aliquots of each sample with known amounts of trace elements to cover five orders of magnitude (0, 1, 10, 50 and 100 ppb). See also Gardner-Vandy et al. (2011) for laboratory technique.

Our measured JB-2 data show good agreement with the reference values within a 2-σ error (Table 2). A few exceptions are noted. Ni is a factor of 5 too high, and Ga, Ge, Cs, Cd, and In are all between a factor of 2–4 too high. We treat our analyses of these elements in Tafassasset with caution. Mo, Zn and Eu are slightly high outside of the 2-σ error, but not enough to cause significant concern. Se is high and Te is low, but these elements have only provisional reference values for JB-2, so we give the disagreement little merit.

2.3. Oxygen isotope analysis

Oxygen isotope analysis was carried out at the Open University using an infrared laser fluorination system (Miller et al., 1999). All analyses were obtained on whole-rock samples (0.5–2 mg). After fluorination, the O_2 released was purified by passing it through two cryogenic nitrogen traps and over a bed of heated KBr. O_2 was analyzed using a Micromass Prism III dual inlet mass spectrometer in the case of the Tafa-MK lithology and using a Thermo MAT 253 instrument in the case of the Tafa-Paris lithology and also for the brachinites NWA 3151 and Hughes 026. Analytical precision (1-σ), based on replicate analysis of international (NBS-28 quartz, UWG-2 garnet) and internal standards, is approximately ±0.04‰ for $\delta^{17}O$; ±0.08‰ for $\delta^{18}O$; ±0.024‰ for $\Delta^{17}O$ (Miller et al., 1999). All sample powders analyzed in this study were drawn from larger homogenized aliquots, obtained by crushing interior whole rock chips, with a minimum mass of about 100 mg. The precision (1-σ) quoted for individual meteorite samples is based on replicate analyses.

Oxygen isotopic analyses are reported in standard δ notation where $\delta^{18}O$ has been calculated as: $\delta^{18}O = [(^{18}O/^{16}O_{sample}/^{18}O/^{16}O_{ref}) - 1] \times 1000$ per mil (‰) and similarly for $\delta^{17}O$ using the $^{17}O/^{16}O$ ratio. $\Delta^{17}O$, which represents the deviation from the terrestrial fractionation line, has been calculated using the linearized format of Miller (2002):

$$\Delta^{17}O = 1000 \ln(1 + \delta^{17}O/1000) - \lambda 1000 \ln(1 + \delta^{18}O/1000)$$

where $\lambda = 0.5247$.

Table 2
Major and trace element abundances for JB-2 reference basalt.

Z	Element	Units	Measured value		Reference value[a]	
			Conc.	1σ	Conc.	1σ
11	Na	μg/g	15,200	260	15,100	
12	Mg	μg/g	29,300	450	27,862	
13	Al	μg/g	87,700	1560	77,400	
15	P	μg/g	380	8	440	
16	S	μg/g			17.9	6.2
19	K	μg/g	2900	74	3500	
20	Ca	μg/g	72,100	1300	70,200	
21	Sc	μg/g	49.2	3	53.5	6.6
22	Ti	μg/g	6240	180	7133	
23	V	μg/g	570	8	575	36
24	Cr	μg/g	29.9	0.9	28.1	5.3
25	Mn	μg/g	1920	95	1690	
26	Fe	μg/g	111,900	1424	99,600	
27	Co	μg/g	42.5	1.4	38	6.6
28	Ni	μg/g	77	10	16.6	6.7
29	Cu	μg/g	219	4	225	16
30	Zn	μg/g	139	4	108	11
31	Ga	μg/g	27.9	0.6	17	2.7
32	Ge	μg/g	2.9	0.1	1.35	0.32
33	As	μg/g	3.48	0.2	2.87	0.85
34	Se	μg/g	0.31	0.07	*0.19*	*0.075*
37	Rb	μg/g	8.12	0.17	7.37	2.89
38	Sr	μg/g	172	3	178	19
39	Y	μg/g	21.5	0.6	24.9	3.1
40	Zr	μg/g	44.7	0.42	51.2	6.1
41	Nb	μg/g	0.92	0.05	*1.58*	*1.09*
42	Mo	μg/g	2.39	0.02	1.08	0.47
48	Cd	μg/g	0.493	0.03	0.14	0.0051
49	In	μg/g	0.321	0.05	0.094	0.03
50	Sn	μg/g	0.11	0.002	0.95	0.44
52	Te	μg/g	0.2	0.009	*4*	
55	Cs	μg/g	1.78	0.17	0.85	0.2
56	Ba	μg/g	204	2.1	222	31
57	La	μg/g	2.58	0.143	2.35	0.23
58	Ce	μg/g	6.235	0.189	6.76	0.95
59	Pr	μg/g	1.38	0.008	1.01	0.26
60	Nd	μg/g	6.62	0.098	6.63	0.7
62	Sm	μg/g	2.437	0.055	2.31	0.37
63	Eu	μg/g	1.219	0.024	0.86	0.07
64	Gd	μg/g	2.59	0.18	3.28	0.31
65	Tb	μg/g	0.853	0.021	0.6	0.1
66	Dy	μg/g	4.107	0.082	3.73	0.59
67	Ho	μg/g	1.079	0.05	0.75	0.17
68	Er	μg/g	2.686	0.077	2.6	0.3
69	Tm	μg/g	0.567	0.014	0.41	0.1
70	Yb	μg/g	2.677	0.068	2.62	0.4
71	Lu	μg/g	0.535	0.04	0.4	0.06
72	Hf	μg/g	1.86	0.061	1.49	0.31
75	Re	μg/g	0.28	0.055	*0.38*	
82	Pb	μg/g	5.45	0.2	5.36	1.08
90	Th	μg/g	0.46	0.064	0.35	0.17
92	U	μg/g	0.35	0.05	0.18	0.067

All reference values are recommended values except those in italics.
[a] Reference values from Imai et al. (1995).

2.4. Thermodynamic calculations

We used the methodology of Benedix et al. (2005) to calculate the thermodynamic environment, i.e. the oxygen fugacity (fO_2), for the formation of Tafassasset. To do this, we used the FeO content of olivine and pyroxene, where the relationship between mineral composition and fO_2 are given by the following reactions:

$$2Fe + SiO_2 + O_2(g) = Fe_2SiO_4 \quad QIFa \tag{1}$$

$$Fe + SiO_2 + \frac{1}{2}O_2(g) = FeSiO_3 \quad QIFs \tag{2}$$

Here, Fe_2SiO_4 is fayalite, QIFa is the quartz–iron–fayalite system, $FeSiO_3$ is ferrosilite, and QIFs is the quartz–iron–ferrosilite system. Solving these reactions for the equilibrium constant (K) relates reactions (1) and (2) to temperature (T) as:

$$\log K_1 = \log\left(\frac{a_{Fa}}{a_{Fe}^2 \cdot a_{SiO_2} \cdot fO_2}\right) = \frac{29592}{T} - 7.61 \tag{3}$$

$$\log K_2 = \log\left(\frac{a_{Fs}}{a_{Fe} \cdot a_{SiO_2} \cdot fO_2^{1/2}}\right) = \frac{29634}{T} - 7.60 \tag{4}$$

which are valid between $773\ K \leqslant T \leqslant 1373\ K$. Here, a_{Fa} is the activity of fayalite, a_{Fs} is the activity of ferrosilite, a_{Fe} is the activity of Fe metal, and a_{SiO_2} is the activity of silica.

We calculated the two closure temperatures for each meteorite using the olivine–chromite and two-pyroxene mineral thermometers. We used a supplemental applet of MELTS to find the olivine–chromite temperature (Sack and Ghiorso, 1991a,b; M. Ghiorso, personal communication) and the program QUILF to find the two-pyroxene temperature (Anderson et al., 1993), using mineral assemblages of contacting phases for each mineral pair. We calculated the a_{Fe} from the average composition of individual metal grains in Tafassasset and used the online MELTS calculator to find the activity of fayalite and ferrosilite (Sack and Ghiorso, 1989; Hirschmann, 1991). As done by Benedix et al. (2005), we assumed $a_{SiO_2} = 0.9$. All calculations were performed at 1 bar which is a reasonable proxy for an asteroid-sized body.

3. RESULTS

3.1. Petrography

Hand samples of Tafa-MK and the large 3.93 gram chip of Tafa-Paris reveal a dark gray stony meteorite with metal blebs that range from sub-millimeter to several millimeters in longest dimension and vary in shape from round to subrounded. All exhibit minimal weathering (weathering grade W0/1 on the Wlotzka (1993) weathering scale of ordinary chondrites). Fig. 1 is a view of the Tafa-Paris5,2 thin section in cross-polarized transmitted light and shows Tafassasset's recrystallized, equigranular texture. The dominant mineral is birefrengent olivine that occurs as subhedral to anhedral grains which often meet at 120° triple junctions. Large (>1 mm) low-Ca pyroxene grains often poikilitically enclose rounded olivine and high-Ca pyroxene grains. The opaque minerals in Fig. 1 are metal and sulfide identified under reflected light.

Fig. 2 gives three views (two 3-color combined X-ray element maps and a back-scattered electron (BSE) image) of portions of the Tafa-MK1 and Tafa-MK2 thin sections. The mineralogy shown in Fig. 2a–b is representative of the rest of the thin sections. Fig. 2a shows the high abundance of olivine (green phase) and a heterogeneous distribution of low- and high-Ca pyroxene (light and medium blue, respectively). Chromite (dark red) occurs interstitial to the mafic silicates. Fig. 2b shows the occurrence of metal (low-Ni is pink; high-Ni is purple) and sulfide (bright green) in the same region. While olivine, metal and sulfide are ubiquitous throughout the sample, pyroxene and plagioclase are not, leaving areas that are either enriched or depleted in these minerals. Low-Ca pyroxene (the light blue phase in Fig. 2a) occurs as large (>1 mm) rounded areas that poikilitically enclose olivine and high-Ca pyroxene.

Fe,Ni-metal grains vary in size from ~10 μm to over 3 mm in longest dimension (Fig. 2c). Many of the larger (>~400 μm) metal grains exhibit plessite texture, similar to duplex plessite described by Buchwald (1975). Plessite is a mixture of kamacite, taenite, and/or tetrataenite and forms by the decomposition of martensite during low-temperature metamorphism (Goldstein and Michael, 2006; Kimura et al. 2008). The largest of the grains (those >~1 mm) contain a decomposed Widmanstätten pattern that is easily seen in the BSE image but not in the 3-color element map (Fig. 2). This is clearly viewable in Fig. 2c in

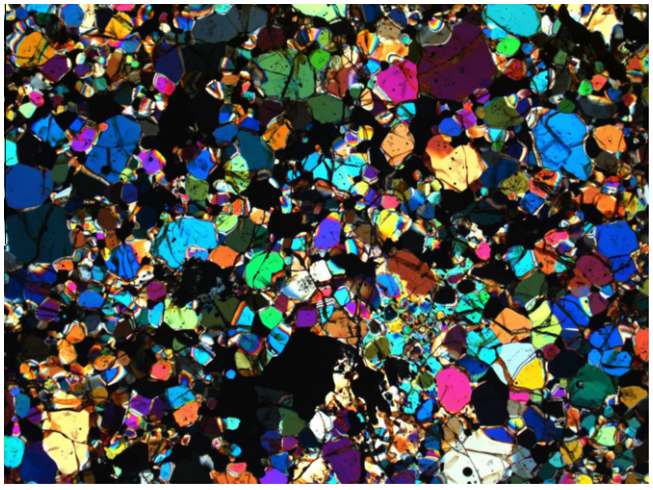

Fig. 1. Cross-polarized light image of an area in the Tafa-Paris 5, 2 thin section. Field of view is 2.77 mm by 2.09 mm. Birefrengent mineral is olivine; opaque minerals are metal and sulfide.

the largest metal grain (3.3 mm in longest dimension) of the seven thin sections.

The modal abundances of the phases in all Tafassasset thin sections examined are given in Table 3 along with abundances averaged for the combined area of the sections.

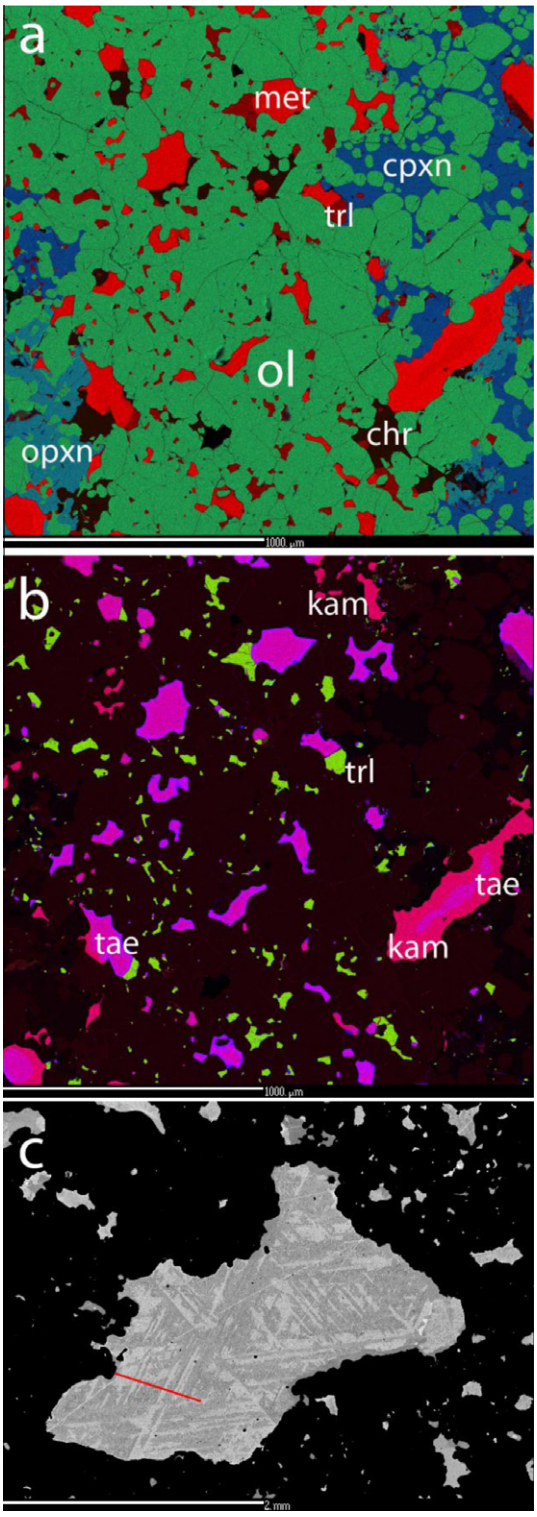

Even though olivine is the dominant phase in the seven thin sections (an average of ~58 vol.%), there is marked heterogeneity in the proportions of the remaining phases, specifically plagioclase, metal and sulfide. This heterogeneity across all the thin sections is consistent with the heterogeneity seen internally in each thin section.

Fig. 3a–b shows two back-scattered electron (BSE) images of Tafassasset from Tafa-MK1 and Tafa-Paris3 thin sections, respectively. Fig. 3a shows an area representative of the mineral modes and textures in Tafassasset. Olivine is the dominant phase in the image, and plagioclase and both high- and low-Ca pyroxene occur interstitial to the olivine. Metal, sulfide, chromite and phosphate grains occur either interstitially to the olivine or as separate grains. Fig. 3b shows a representative view of a pyroxene-rich area, with a large low-Ca pyroxene grain poikilitically enclosing olivine. In both of these BSE images, plagioclase is seen surrounding metal and sulfide, and plagioclase and pyroxene frequently poikilitically enclose olivine. As shown in Figs. 2c and 3b, large ($\geqslant$500 μm) grains of metal are common in Tafassasset. Some metal gains are isolated, while others occur interstitially with irregular sub-rounded borders.

The textures described here for the Tafa-MK1 thin section are very similar to those found in the other six thin sections analyzed. Despite the report of such features by Bourot-Denise et al. (2002) and Bunch et al. (2005), we did not find relict chondrules in the seven thin sections analyzed. This could be due to heterogeneity of the sample as a whole and/or rarity of the relict chondrules.

3.2. Mineral compositions

Analyses of olivine reveal homogeneous composition with an average of $Fa_{29 \pm 0.6}$. There is no detectable NiO in any of the olivine grains. CaO content varies from undetectable to 0.07 wt.%, and Cr_2O_3 varies from undetectable

Fig. 2. Three views of a portion of the Tafa-MK1 thin section: (a) a 3-color combined X-ray map of a region of the Tafa-MK1 thin section with representative mineralogy. Fe is on the red channel, Mg on the green channel, and Si on the blue channel. Phases marked on the image are "met" for Fe,Ni-metal, "trl" for troilite, "cpxn" for high-Ca pyroxene, "ol" for olivine, "opxn" for low-Ca pyroxene, and "chr" for chromite. Any black phase is either phosphate or a void; (b) a 3-color combined X-ray map of the same representative region in the Tafa-MK1 thin section as Fig. 2a. Fe is on the red channel, S on the green channel, and Ni on the blue channel. Phases marked on the image are "kam" for kamacite, "tae" for taenite or tetrataenite, and "trl" for troilite. In this image, the more Ni there is in the metal phase, the more purple it appears; (c) a back-scattered electron (BSE) image of a large metal grain in the Tafa-MK1 thin section showing a Widmanstätten pattern. Red line denotes location of Line A. Note: all original X-ray maps and BSE images were stretched (levels, contrast, and brightness) in Adobe Photoshop in order to better show the chemical variations; the images should not be used for quantitative compositional information.

Table 3
Modal mineralogy of Tafassasset thin sections.

	Tafa-MK TS1	Tafa-MK TS2	Tafa-MK TS3	Tafa-MK TS4	Tafa-Paris3	Tafa-Paris5,2	Tafa-Paris5,4	Area avg. abund. Total area:
Area (mm^2)	230	242	250	243	114	111	168	1358 mm^2
Olivine	52.7	68	51	61.8	49.1	63.2	54	57.5
Pyroxene	23.1	16.5	33.3	20.4	29.6	22.3	29.8	24.6
Plagioclase	1	2.2	3.3	3.3	5.9	3.9	4.2	3.1
Fe,Ni-metal	14	10.4	8	9.8	12.4	7.5	9.8	10.3
Sulfide	7	1.1	2.6	3.1	2	2.1	1.6	3
Chromite	2	0.6	1.1	0.9	0.5	0.5	0.3	0.9
Phosphate	0.2	1.2	0.7	0.7	0.5	0.5	0.3	0.6
Total	100	100	100	100	100	100	100	100

to 0.07 wt.%. Pyroxene compositions are also homogeneous, with an average composition of $Fs_{24 \pm 0.6}En_{73 \pm 1}Wo_{3.7 \pm 0.9}$ for low-Ca pyroxene and $Fs_{12 \pm 0.6}En_{49 \pm 0.7}Wo_{39 \pm 1}$ for high-Ca pyroxene (Fig. 4). These average two pyroxene compositions correspond to an equilibration temperature of 1073 ± 37 °C (Anderson et al., 1993). Plagioclase composition spans a continuous range in Ca and Na content between An_{23} and An_{47} (Fig. 5). A composition of An_{47} corresponds to a peak temperature of 1270 °C on the binary albite-anorthite phase diagram (Morse, 1994). Average compositions of olivine, pyroxene and plagioclase grains in Tafassasset are given in Table 4.

Fe,Ni-metal grains span a continuous range in composition between 5.3 and 43 wt.% Ni. As shown in Fig. 2b, metal grains are often zoned in Ni-content to varying degrees. Fig. 6 details the Ni composition across two line scans, one across the large 3.3 mm metal grain with a decomposed Widmanstätten pattern (Fig. 2c) and one across a ~1.4 mm grain not shown. Each metal grain has a low-Ni (~6 wt.%) rim and variable Ni-content interior in the region with plessite texture. Most EMPA points on the decomposed pattern yield metal with 5–7 wt.% Ni, yet there are Ni-rich areas that have 11–43 wt.% Ni (Fig. 2c). There is no discernable "M" profile in either to calculate a cooling rate from the Widmanstätten pattern. Sulfide grains are troilite, with 0.04–0.34 wt.% Cr. Chromites have 8.0–9.4 wt.% Al_2O_3 and 3.2–4.5 wt.% MgO. Average compositions of metal and sulfide are given in Table 5, and an average composition for the chromite grains in Tafassasset is given in Table 6.

The mineral compositions given here are consistent across the seven thin sections.

3.3. Bulk chemistry

Major, minor and trace element data for the three chips of Tafassasset measured by ICP-MS are given in Table 7. The major and minor element concentrations in the three Tafassasset chips reflect the heterogeneity of the mineral modes given in Table 3. The Tafa-MKb chip has much less Na than the other two chips, but this depletion is likely due to undersampling of plagioclase as the Na depletion correlates with depletion in other plagioclase elements (e.g. Al and K) in the same chip. The Tafa-MKb chip is also depleted in refractory lithophile elements like Mg, Ca, Sc, and Mn that go into olivine and pyroxene. This sample likely had a higher portion of metal and sulfide than the other two chips. The marked enrichment in Fe, Ni, and Co confirms this. Tafa-Paris5 has more Ti, V, and Cr than the other two samples, likely because of oversampling of chromite compared to the other two chips.

Fig. 7 contains volatility trend diagrams for the three chips of Tafassasset. Tafa-MKa and Tafa-MKb display similar patterns and are depleted in many lithophile and siderophile elements and all the chalcophile elements. Noteworthy exceptions are the enrichment of Fe, Ni, Co, and Mo, as well as Re for Tafa-MKb. (As noted above, our Ni measurement of the JB-2 standard was a factor of 5 high compared to the reference value for JB-2. Because the Ni values determined for the three Tafassasset stones are similar to the Ni data reported by Zipfel et al. (2002), we consider our analyses accurate.) Tafa-Paris5 is slightly depleted or chondritic in most lithophile and siderophile elements and depleted in all chalcophile elements. It has no marked enrichment in Fe, Ni or Co, yet it does have a slight enrichment in Re and Mo. In general, the refractory lithophile and siderophile element composition of Tafassasset is slightly fractionated from CI chondrites.

The rare earth element (REE) patterns for the three chips are shown in Fig. 8. REE patterns vary slightly between the chips, possibly due to sampling bias of silicate minerals and phosphate. All three are slightly depleted in REEs relative to CI chondrites, but the degree of that depletion varies. While both Tafa-MKa and Tafa-MKb show enrichments in light REEs (LREEs), this enrichment is more pronounced in Tafa-MKb. Tafa-MKa has no Eu anomaly and Tafa-MKb has a slight negative Eu anomaly. Tafa-Paris5 is slightly depleted in LREE and has a positive Eu anomaly. The heavy REEs (HREEs) approach chondritic values for Tafa-Paris5.

Fig. 9 shows the three Tafassasset chips on a CI-normalized Se/Co vs. Na/Sc plot. These elemental ratios are theoretical proxies for the troilite/metal and plagioclase/pyroxene component of the samples analyzed. As discussed by Mittlefehldt et al. (1998), partial melting of a chondritic source will move from a pure CI-chondritic composition (at the crossing of the two dashed lines) to a depleted composition (the lower left) as the removal of Fe,Ni–FeS and basaltic partial melt occurs. The three Tafassasset samples

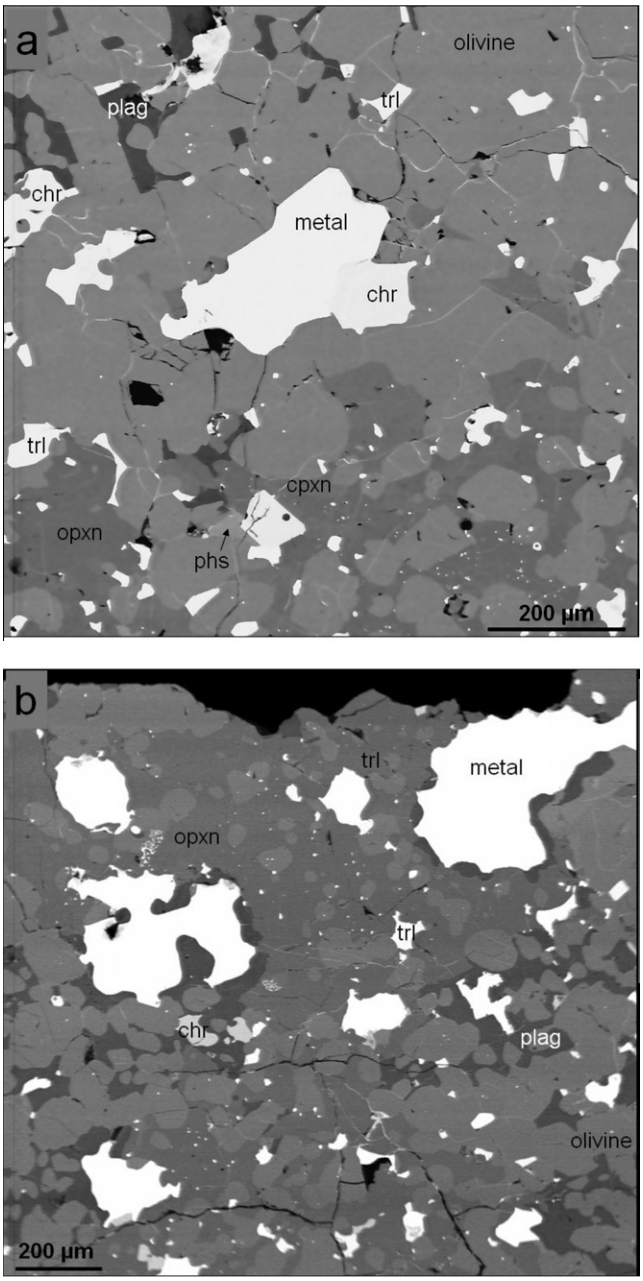

Fig. 3. Backscattered electron images of (a) Tafa-MK1 and (b) Tafa-Paris3. Mineral abbreviations are: "opxn" for low-Ca pyroxene, "cpxn" for high-Ca pyroxene, "plag" for plagioclase, "trl" for troilite, "chr" for chromite, and "phs" for phosphate.

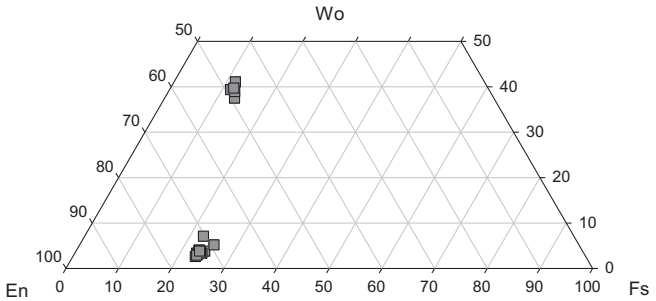

Fig. 4. Truncated pyroxene quadrilateral showing Tafassasset pyroxene.

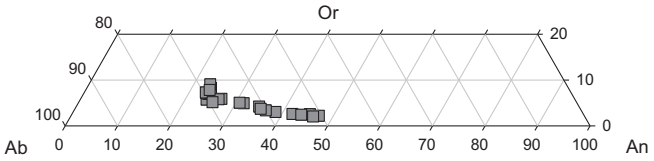

Fig. 5. Truncated plagioclase quadrilateral showing Tafassasset plagioclase.

Table 4
Average compositions of representative olivine, pyroxene, and plagioclase grains from Tafassasset (wt.% oxides).

	Olivine		Low-Ca pyroxene		High-Ca pyroxene		Plagioclase	
	avg	std	avg	std	avg	std	avg	std
N	34		10		5		26	
SiO_2	37.49	0.28	54.49	0.23	53.28	0.41	59.38	2.00
TiO_2	bdl		0.20	0.03	0.40	0.03	bdl	
Al_2O_3	bdl		0.49	0.07	0.96	0.18	25.24	1.53
Cr_2O_3	bdl		0.40	0.10	0.92	0.18	bdl	
FeO	25.78	0.47	15.48	0.21	8.08	1.27	0.61	0.39
MnO	0.42	0.02	0.41	0.02	0.26	0.03	bdl	
MgO	36.33	0.46	26.86	0.42	17.79	1.97	bdl	
CaO	0.05	0.01	1.84	0.21	17.84	2.87	6.51	1.82
NiO	bdl		bdl		bdl		nd	
Na_2O	bdl		bdl		0.43	0.09	7.37	0.85
K_2O	bdl		bdl		bdl		0.93	0.39
Total	100.07		100.17		99.95		100.05	
Molar Fe/Mn, 100 × Mg/(Mg + Fe) and mole percent mineral end members.								
Fe/Mn	61.9	2.9						
Fa	28.6	0.6						
Fs, An			23.6	0.6	12.2	0.6	32	9
En, Ab			72.6	1	48.5	0.7	62.9	7
Wo, Or			3.7	0.9	39.3	1	5.1	2

plot in the lower left of the diagram, indicating that all have lost both Fe,Ni–FeS and some basaltic melt component, at least on the scale of the sample size. Three brachinites and the LEW 88763 and Divnoe ungrouped primitive achondrites also plot in this region. Included on the plot for reference is average CR chondrite, which is depleted with respect to both Se/Co and Na/Sc compared to the CI chondrites. We include this point in effort to simply show that the interpretation of this plot is different with CR-like starting composition. When compared to the CR-chondrite point, only the Tafa-MKb sample lost both Fe,Ni–FeS and a basaltic melt component; the Tafa-MKa and Tafa-Paris5 samples lost only the sulfide component. Thus, a difference in precursor material denotes a slightly different interpretation of this plot.

3.4. Oxygen isotopes

The two distinct Tafassasset lithologies analyzed at the Open University (Table 8, Fig. 10) are within error of each other and plot just outside the acapulcoite–lodranite field, but well within the field of CR chondrites. Two additional oxygen isotope analyses of Tafassasset have been undertaken by other groups (Russell et al., 2002) (Fig. 10). The Tafassasset lithology (Tafa-Paris) described by Bourot-Denise et al. (2002) plots within both the acapulcoite–lodranite and CR chondrite fields (Fig. 10). In contrast, the analysis of Clayton and Mayeda (Tafa-Freiburg), undertaken on a distinct stone classified by J. Otto (Russell et al., 2002), plots away from the acapulcoite–lodranite field, well within the field defined by CR chondrite analyses (Fig. 10). Taken at face value, these analyses suggest that Tafassasset displays a significant level of oxygen isotope heterogeneity. However, in view of the almost identical analyses obtained on the two fractions analyzed at the Open University, it is also possible that some of this variation reflects differing analytical procedures (i.e. laser fluorination versus heated Ni bombs, varying oxygen yields, differences in working gas calibration).

In view of the suggestion that Tafassasset is a brachinite-like meteorite (Nehru et al., 2003), we have also undertaken a limited study of two brachinites NWA 3151 and Hughes 026. Our new analyses of NWA 3151 and Hughes 026 plot within the main brachinite field in Fig. 10 and are in good agreement with previous analyses of these samples (Irving et al., 2005; Greenwood et al., 2007). Despite their mineralogical and petrographic similarities (Nehru et al., 2003), the distinct oxygen isotope compositions of Tafassasset and the brachinites (including NWA 3151 and Hughes 026) precludes any direct genetic link between them. In contrast, Tafassasset plots close to the anomalous brachinite LEW 88763 (Fig. 10). The possibility of a genetic link between these meteorites is discussed further in Section 4.

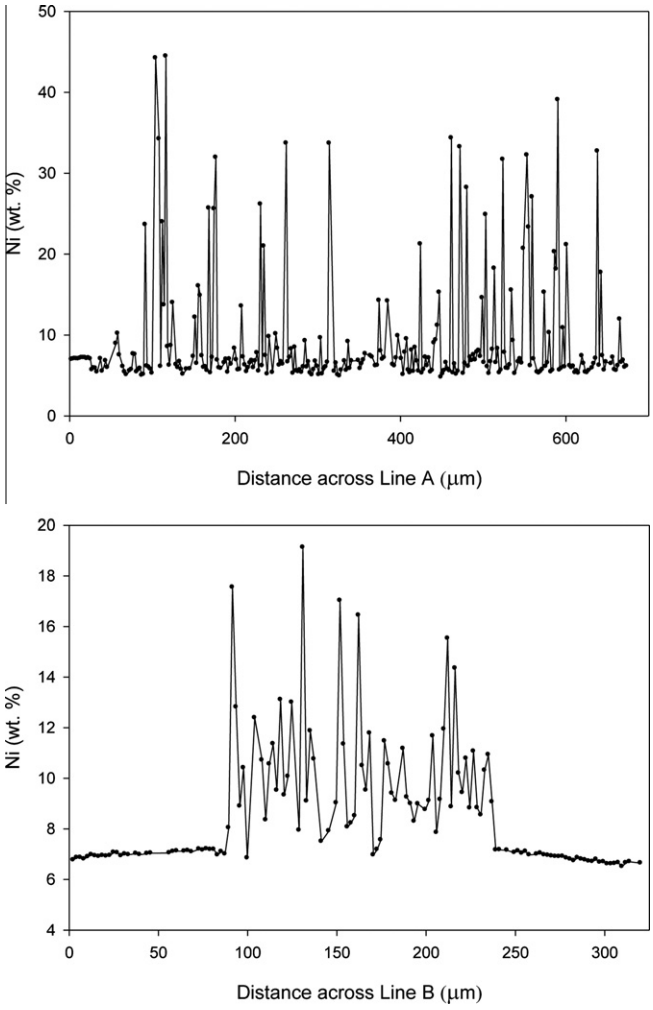

Fig. 6. Line scans across two Fe,Ni-metal grains in Tafassasset. Line A is shown in Fig. 2c; Line B is not shown on an image.

Table 5
Average compositions of representative metal and troilite grains from Tafassasset (wt.% element).

	Metal		Troilite	
	avg	std	avg	std
N	203		92	
Fe	89.16	3.46	63.20	0.31
Ni	9.90	3.48	bdl	
Co	0.576	0.086	bdl	
S	bdl		36.67	0.18
Cr	bdl		0.053	0.045
Total	99.64		99.92	

Table 6
Average composition of representative chromite grains from Tafassasset (wt.% oxides).

	avg	std
N	13	
SiO_2	0.095	0.022
TiO_2	2.58	0.17
Al_2O_3	8.55	0.61
V_2O_3	0.577	0.078
Cr_2O_3	54.18	0.45
FeO	29.60	0.54
MnO	0.841	0.042
MgO	3.830	0.317
Total	100.26	

3.5. Thermodynamic calculations

We calculated two fO_2 values for Tafassasset using reactions (3) and (4) given above and the olivine–chromite and two-pyroxene thermometers, respectively. An average of calculated olivine–chromite and 2-pyroxene closure temperatures are given in Table 9, along with the calculated fO_2 (in relation to the iron–wüstite buffer) for each mineral pair. The mineral assemblages utilized for this calculation were co-existing mineral pairs from the Tafa-MK1 and Tafa-Paris3 thin sections. We analyzed line scans along individual grains using the electron microprobe to check for homogeneity. Both the olivine–chromite and 2-pyroxene closure temperatures for Tafassasset are above the Fe,Ni–FeS eutectic temperature of 950 °C, and the 2-pyroxene temperatures, within error, reach the lower limit of generation of a basaltic melt in chondritic

Table 7
Bulk chemical data for Tafassasset by ICP-MS.

Z	Element	units	Tafa-MKa		Tafa-MKb		Tafa-Paris5	
			Conc.	1σ error	Conc.	1σ error	Conc.	1σ error
11	Na	μg/g	2280	65	350	11	2840	75
12	Mg	wt.%	12.4	0.16	9.7	0.14	12.9	0.39
13	Al	μg/g	4490	60	965	11	7570	323
15	P	μg/g	400	4	340	3	510	5
16	S	μg/g	6970	52	8430	51	nd	
19	K	μg/g	250	4	46	1	nd	
20	Ca	μg/g	5120	83	2660	42	9470	114
21	Sc	μg/g	7.6	0.14	5.9	0.14	8.4	0.16
22	Ti	μg/g	220	2	200	1	430	9
23	V	μg/g	38	1	36	1	72	1
24	Cr	μg/g	1580	113	1800	21	2850	38
25	Mn	μg/g	1910	25	1510	13	1850	12
26	Fe	wt.%	28.5	0.21	40.4	0.42	23.0	0.24
27	Co	μg/g	1200	7	2270	23	680	6
28	Ni	wt.%	2.02	0.03	3.27	0.043	1.20	0.0043
29	Cu	μg/g	91	1	141	2	137	3
30	Zn	μg/g	17	0.3	18	0.2	nd	
31	Ga	μg/g	1.98	0.043	2.93	0.039	2.35	0.008
32	Ge	μg/g	3	0.21	4.3	0.3	9.2	0.73
34	Se	μg/g	7.52	1.5	7.41	1.5	1.50	0.60
37	Rb	μg/g	1.2	0.02	0.62	0.02	1.08	0.03
38	Sr	μg/g	7.27	0.12	4.36	0.07	8.39	0.12
39	Y	μg/g	0.63	0.01	0.31	0.004	1.34	0.03
40	Zr	μg/g	5.76	0.23	6.00	0.24	5.19	0.09
41	Nb	μg/g	0.41	0.01	0.38	0.01	0.31	0.002
42	Mo	μg/g	2.1	0.05	3.6	0.09	1.8	0.16
48	Cd	μg/g	0.043	0.004	0.039	0.006	0.045	0.003
49	In	μg/g	bdl		bdl		0.029	0.002
50	Sn	μg/g	0.21	0.004	0.59	0.027	bdl	
52	Te	μg/g	bdl		0.014	0.001	0.024	0.002
55	Cs	μg/g	0.067	0.002	0.062	0.001	0.023	0.001
56	Ba	μg/g	4.35	0.12	2.20	0.048	3.45	0.091
57	La	μg/g	0.114	0.008	0.093	0.008	0.144	0.025
58	Ce	μg/g	0.377	0.009	0.284	0.007	0.361	0.017
59	Pr	μg/g	0.053	0.001	0.037	0.001	0.049	0.004
60	Nd	μg/g	0.258	0.009	0.167	0.003	0.286	0.014
62	Sm	μg/g	0.074	0.004	0.043	0.003	0.103	0.003
63	Eu	μg/g	0.025	0.004	0.010	0.003	0.059	0.001
64	Gd	μg/g	0.087	0.018	0.048	0.009	0.129	0.012
65	Tb	μg/g	bdl		bdl		0.032	0.003
66	Dy	μg/g	0.111	0.017	0.047	0.008	0.224	0.006
67	Ho	μg/g	0.016	0.003	0.011	0.002	0.050	0.003
68	Er	μg/g	0.049	0.014	0.034	0.010	0.152	0.006
69	Tm	μg/g	0.010	0.003	0.004	0.002	0.023	0.001
70	Yb	μg/g	0.081	0.020	nd		0.160	0.007
71	Lu	μg/g	nd		nd		0.021	0.0003
72	Hf	μg/g	0.18	0.01	0.18	0.01	0.17	0.02
75	Re	μg/g	0.03	0.001	0.11	0.002	0.08	0.002
82	Pb	μg/g	0.9	0.02	0.3	0.006	0.05	0.003
90	Th	μg/g	0.12	0.01	0.16	0.01	0.02	0.004
92	U	μg/g	0.01	0.001	0.01	0.0004	0.03	0.004

nd: not determined, often due to error with either signal or blank that made concentration too low to discern; bdl: below detection limit, listed for data that is $\leqslant 2\times$ the detection limit.

starting composition (~1050 °C) (Kushiro and Mysen, 1979; Takahashi, 1983). Thus, a partial melt was likely generated in the Tafassasset parent body. The fO_2 calculated from the olivine–chromite mineral pair is IW-1.2, and the fO_2 calculated from the 2-pyroxene pair is IW-1.

4. DISCUSSION

The results of our petrographic and geochemical analyses of four distinct stones of Tafassasset indicate that the Tafassasset name is given to one heterogeneous meteorite

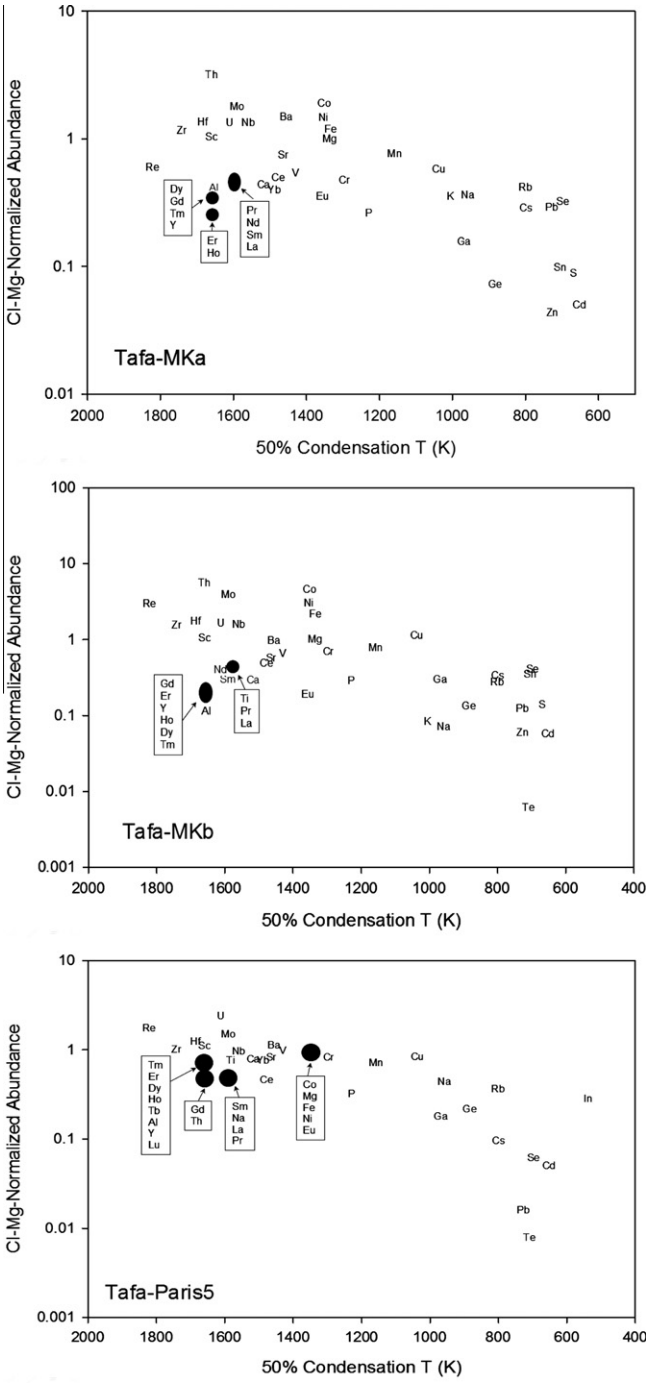

Fig. 7. Volatility trend diagrams for the three Tafassasset chips analyzed by ICP-MS.

and not to separate meteorites that were collected with the same name. This study yields strong evidence indicating the Tafassasset meteorite underwent partial melting on its parent body. All of the thin sections analyzed show a recrystallized meteorite with heterogeneous distribution of mineral phases which varies on a thin-section scale, especially high-Ca pyroxene and plagioclase. These two minerals, the first silicates to become part of a silicate melt, show redistribution expected during the partial melting process. This small-scale distribution indicates a low-degree of partial melting and variable amounts of melt migration across the stones. The large variation in plagioclase composition, like that reported in the lodranite primitive achondrites, provides further evidence of partial melting (McCoy et al., 1997). Likewise, the mineral-pair closure temperatures calculated prove that Tafassasset witnessed temperatures high enough to generate both an Fe,Ni–FeS and silicate partial melt. Once partial melting took place, Tafas-

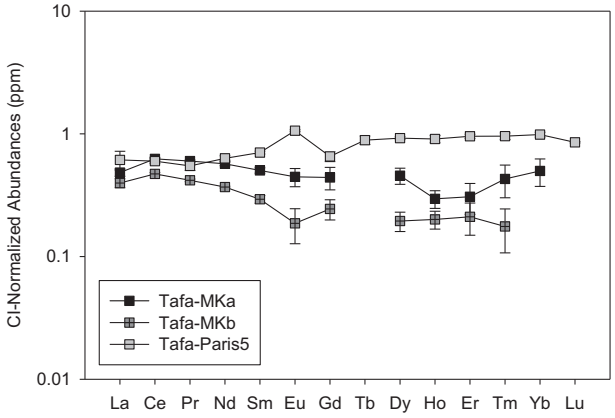

Fig. 8. Rare Earth Element plot for 3 Tafassasset chips analyzed by ICP-MS.

Table 8
Oxygen isotope data for Tafassasset.

	$\delta^{17}O‰$	2σ	$\delta^{18}O‰$	2σ	$\Delta^{17}O‰$	2σ
TafaMK	−0.40		2.25		−1.58	
TafaMK	−0.42		2.24		−1.59	
Mean	−0.41	0.02	2.25	0.02	−1.59	0.01
Tafa-Paris5	−0.39		2.24		−1.56	
Tafa-Paris5	−0.25		2.52		−1.57	
Mean	−0.32	0.2	2.38	0.4	−1.56	0.01
Hughes 026	1.97		4.11		−0.19	
NWA 3151	2.04		4.19		−0.16	
Tafa-Paris[a]	0.18	0.16	2.94	0.40	−1.36	
Tafa-Freiburg[b]	−0.85		1.70		−1.74	

[a] Tafa-Paris data from Russell et al. (2002) and reported in Bourot-Denise et al. 2002.
[b] Tafa-Freiburg data from Russell et al. (2002).

sasset cooled slowly in order for a Widmanstätten pattern to form in the large metal grains. Trace element composition shows clear depletions in incompatible elements that would be mobilized during the partial melting process. It still remains unknown, however, if the precursor rock is sampled in the current meteorite collection. In the following sections, we compare Tafassasset to other meteorite groups in order to provide insight concerning the composition of the precursor rock.

4.1. Comparison to other meteorite groups and classification

Tafassasset has been linked and compared to two groups of meteorites: (1) the CR chondrites because of its oxygen isotope composition, similar metal abundance to the CR chondrites, and reported relict chondrules similar in mineralogy and morphology to those in Renazzo (Bourot-Denise et al., 2002), and (2) the primitive achondrites because of a metal-free renormalized mineralogy similar to Brachina and depleted refractory lithophile element composition similar to the brachinites and other primitive achondrites (Zipfel et al., 2002; Nehru et al., 2003). In the following section, we will compare Tafassasset to these two groups of meteorites in effort to establish its classification and better understand its history. Table 10 gives a list of significant petrologic and geochemical properties of Tafassasset alongside those of ungrouped primitive achondrites LEW 88763 and Divnoe, several brachinites, and the CR chondrites for reference.

The overall petrography, textures, and mineral modes in Tafassasset are most similar to the brachinites and primitive achondrites like Divnoe and LEW 88763 (Table 10). A recrystallized texture with abundant olivine is evident in all these meteorites, as well as in Tafassasset. The mineralogical heterogeneity in Tafassasset is not shared by the brachinites but can easily be explained by the meteorites undergoing different degrees of melt generation and removal. Tafassasset did not undergo as great a degree of partial melting as the brachinites and Divnoe, thus it retained a heterogeneous texture and mineralogy on a thin-section scale. Because we did not find relict chondrules in Tafassasset, we cannot compare that texture to the CR

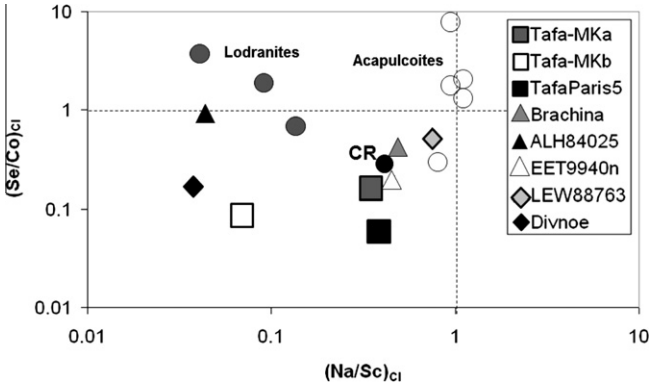

Fig. 9. Se/Co vs. Na/Sc plot for primitive achondrites, Tafassasset, and mean CR chondrite. Tafassasset data is from this work. Data for: Brachina from Nehru et al. (1983); Allan Hills (ALH) 84025 from Warren and Kallemeyn (1989); Elephant Moraine (EET) 9940n is an average of data for EET 99402 and EET 99407 from Mittlefehldt et al. (2003); LEW 88763 from Swindle et al. (1998); and Divnoe from Petaev et al. (1994); mean CR from Kallemeyn et al. (1994). As noted in the figure, data for the acapulcoites are given by open circles and for the lodranites by shaded circles (Mittlefehldt et al. (1998)).

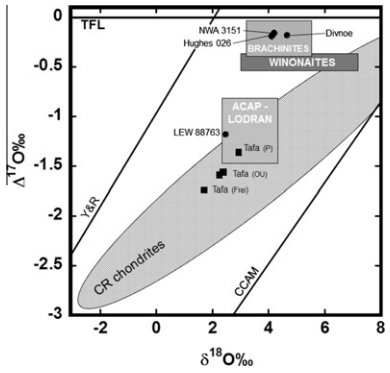

Fig. 10. Oxygen isotope composition of Tafassasset primitive achondrite. Tafassasset samples analyzed for this study are shown by the four black boxes. "Tafa (P)" is data for Tafa-Paris from Bourot-Denise et al. (2002), "Tafa (OU)" is data for Tafa-MK by Open University from this study, and "Tafa (Frei)" is data for Tafa-Freiburg from Russell et al. (2002). Shaded boxes, representing the primitive achondrites, are from Greenwood et al. (2007) and represent the 2-σ variation of the group mean oxygen isotope value for acid-leached fractions. CR chondrite analyses shown in shaded oval are from Clayton and Mayeda (1999) and Schrader et al. (2011). Oxygen isotope analyses of NWA 3151 and Hughes 026 are from this study, Divnoe from Petaev et al. (1994), and LEW 88763 from Greenwood et al. (2007). Reference lines: Y&R: Young and Russell (1998); CCAM: carbonaceous chondrite anhydrous mineral line (Clayton et al., 1977; Clayton and Mayeda, 1999), TFL: terrestrial fractionation line.

chondrites. Tafassasset does have an extraordinary amount of metal compared to the brachinites which contain at most only traces of metal (e.g. Mittlefehldt et al., 2003). Ungrouped primitive achondrites LEW 88763 and Divnoe do contain metal, yet not as much as Tafassasset. Swindle et al. (1998) reported LEW 88763 to be 6% opaque minerals (metal, troilite, and chromite), and Petaev et al. (1994) reported Divnoe to be 9.5% opaque minerals. As given in Table 3, Tafassasset is ~14 vol.% opaque minerals.

Mineral compositions, specifically olivine compositions, are similar to the brachinites, Divnoe, and LEW 88763, and in contrast, the CR chondrites have very reduced mineral compositions (Table 10). Fig. 11 shows a plot of the mole fraction of ferrosilite in orthopyroxene versus the mole fraction fayalite for several chondrite and primitive achondrite groups. Those meteorites that formed in more "reducing" conditions plot on the left side of the diagram, and those that formed in more "oxidizing" conditions plot on the right. The CR chondrites, winonaites, acapulcoites and lodranites have FeO-poor olivine and pyroxene and thus plot on the reduced end, while the brachinites, Divnoe, LEW 88763, and the FeO-rich chondritic meteorites (the CK and R chondrites), plot on the oxidized end. The ordinary chondrites (H, L and LL) are shown for reference. Also noted on this diagram is the fayalite values for the type-I and type-II chondrules in CR chondrites. Type-I chondrules are FeO-poor, and type-II chondrules are FeO-rich and span a wide range of fayalite composition. On this diagram, Tafassasset's olivine and pyroxene compositions plot near those of the brachinites, Divnoe, and LEW 88763 and plot far from those of average CR chondrites (gray oval). With respect to bulk composition, Tafassasset is fractionated from a CI-chondritic composition (Fig. 6) and experienced partial melting, with an Fe,Ni–FeS and a basaltic melt generated and partially removed, at least on the scale of the sample size (Fig. 8). As Fig. 8 demonstrates, this depletion in Se/Co and Na/Sc is seen in the brachinites and primitive achondrites, meteorites that have undergone varying degrees of partial melting and melt removal.

The oxygen isotope composition of Tafassasset, determined both in this and previous studies (Bourot-Denise et al., 2002; Russell et al., 2002), plots well within the field defined by CR chondrite analyses (Clayton and Mayeda, 1999; Schrader et al., 2011) and away from the brachinites and Divnoe (Table 10). Fig. 10 shows all data for Tafassasset along with the CR chondrites and various primitive achondrites. The four Tafassasset points are co-linear in 3-isotope space but do not lie on a mass-dependent fractionation line. The equation for this line is:

$$\delta^{17}O = 0.83 \cdot \delta^{18}O - 2.27 \quad (R^2 = 0.9985)$$

which is slightly different than the CR mixing line calculated by Schrader et al. (2011) which has a slope of

Table 9
Thermodynamic properties of Tafassasset and select winonaites and silicate-rich IAB irons (given in Benedix et al., 2005).

Meteorite[a]	Olivine–chromite temperature (°C)	QIFa[b] log fO_2	ΔIW[c]	Two-pyroxene temperature (°C)	QIFs[d] log fO_2	ΔIW	Δ T[e]
Tafassasset[f]	937	−17.3	−1.2	1073	−15.3	−1.0	99
Winona[g]	674	−24.9	−2.9	994	−17.0	−2.5	320
Caddo county	590	−28.1	−3.0	1016	−17.2	−2.5	426
Campo del Cielo[g]	661	−25.8	−3.1	939	−18.6	−2.6	278
Copiapo	611	−27.4	−3.1	933	−18.8	−2.7	322
Lueders	586	−28.4	−3.2	1067	−16.3	−2.5	481
Udei station	642	−26.2	−2.9	1043	−16.6	−2.3	401

[a] Winona is the type specimen of the winonaites; all else (besides Tafassasset) are sil-IAB irons.
[b] QIFa fO_2 is the fO_2 calculated from the Quartz–Iron–Fayalite system and the olivine–chromite T (K).
[c] ΔIW is the deviation of the calculated fO_2 from the iron–wustite buffer in log units.
[d] QIFs fO_2 is the fO_2 calculated from the Quartz–Iron–Ferrosilite system and the 2-pyroxene T (K).
[e] ΔT is the difference between the olivine–chromite and 2-pyroxene temperatures.
[f] Tafassasset data is an average from the Tafa-MK1 and Tafa-Paris3 thin sections.
[g] Data is the average value given in Benedix et al. (2005).

Table 10
Summary of mineralogical and geochemical data of Tafassasset with select meteorites.

Meteorite	Classification[a]	Olivine (vol.%)	Plagioclase (vol.%)	Metal + sulfide[b] (vol.%)	Olivine (Fa)[c]	O-isotopes ($\Delta^{17}O$)	Ref[d]
Tafassasset	UPA	58	3	13	29	−1.57	1
LEW 88763	UPA	71	10	6	36–37	−1.26	2
Divnoe	UPA	75	1.5	9.5	23–25	−0.26	3
Brachina	Brachinite	80	10	3.3	30	−0.20	4, 5
ALH 84025	Brachinite	79	none	~3	32	−0.32	6, 5
EET 99402	Brachinite	88	5.4	1.3	36	−0.22	7
CR chondrites[e]				6–12	0–6	−2.26	8, 9

[a] UPA: ungrouped primitive achondrite.
[b] For LEW 88763 and Divnoe, this includes chromite (no separate metal and sulfide values were given).
[c] Fa = fayalite content of olivine, calculated as molar (Fe/(Fe + Mg))*100.
[d] References: 1 = this work; 2 = Swindle et al. (1998), 3 = Petaev et al. (1994), 4 = Nehru et al. (1983), 5 = Clayton and Mayeda (1996), 6 = Warren and Kallemeyn (1989), 7 = Mittlefehldt et al. (2003), 8 = Kallemeyn et al. (1994), 9 = Schrader et al. (2011).
[e] Fayalite values for type-I chondrules only.

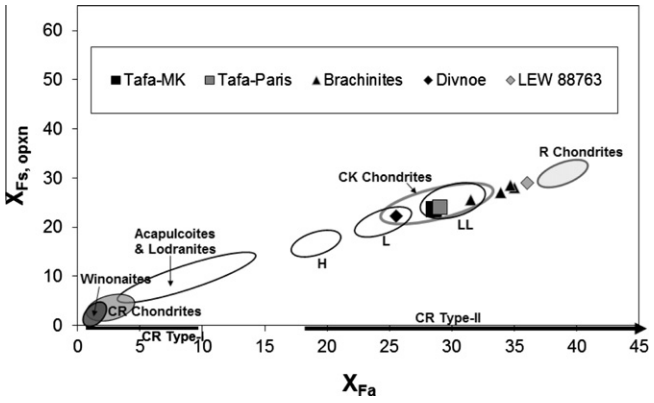

Fig. 11. X_Fs, opxn versus X_Fa plot for various meteorites, showing the winonaites, the CR chondrites, the acapulcoites/lodranites, H, L, and LL ordinary chondrites, Divnoe, the brachinites, LEW 88763, the CK and R chondrites, with Tafassasset. The large arrows on the x-axis denote the field of olivine composition of type-I and type-II chondrules. Data is taken from Nehru et al. (1983), Kallemeyn et al. (1994), Petaev et al. (1994), Mittlefehldt et al. (1998), Swindle et al. (1998) and MetBase (Koblitz 2005).

0.71 ± 0.06. This spread of Tafassasset oxygen isotope analyses could be taken as a reflection of primary heterogeneity within the precursor material. However, as discussed in Section 3, it is not yet clear whether these oxygen isotope differences are real, or reflect varying experimental procedures.

As is clear from Fig. 10, both the acapulcoite–lodranite group and Tafassasset overlap the field of CR chondrites. This relationship suggests that CR-like material may have been a viable precursor to both groups. However, the very clear mineralogical differences between these two sets of primitive achondrites indicate that they formed under very different conditions. It has been suggested by Rubin (2007) that acapulcoites and lodranites formed by shock melting of a CR-like precursor material. This process, however, does not explain the higher modal abundance of Fe,Ni-metal and FeS in the acapulcoite–lodranite meteorites compared to the CR chondrites (Kallemeyn et al., 1994; McCoy et al., 1996). Such a melting process should deplete the CR-like material in FeS, not enrich it.

It has been suggested that Tafassasset is related to the brachinites (Nehru et al., 2003). The oxygen isotope composition of the main group brachinites is distinct from that of Tafassasset and a single asteroidal source for both groups is unlikely. Tafassasset does have an oxygen isotopic composition similar to that of the brachinite-like LEW 88763 and their silicate mineralogy is also broadly similar (Table 10). One important difference between LEW 88763 and Tafassasset is the metal-rich composition of the latter. Tafassasset may represent a precursor stage to the formation of brachinite-like meteorites (LEW 88763, Tafassasset, and Divnoe), where the initial stages of melting have occurred but significant metal separation has not yet taken place. It is clear from Fig. 10 that the oxygen isotopic composition of these meteorites is different, but the brachinites and brachinite-like meteorites share a common characteristic of an olivine dominated, oxidized mineralogy. Rather than indicating a single parent material, this may be indicative of similar formation conditions, i.e. partial melting of a hydrated chondritic precursor material.

There is little data with which to compare Tafassasset's thermodynamic formation conditions except that given by Benedix et al. (2005) for the winonaites and silicate-rich IAB irons and the value modeled for Divnoe by Petaev

et al. (1994). As Fig. 11 clearly shows, the winonaites (and hence silicate-rich IAB irons) formed under much more reducing conditions than the brachinites and primitive achondrites, so it is not surprising that the fO_2 calculated by Benedix et al. (2005) for these meteorites is much lower (~IW-2.5 to IW-3) than that calculated here for Tafassasset (~IW-1) (Table 9). The Divnoe ungrouped primitive achondrite is more similar to Tafassasset in mineral composition and texture (as discussed above), so the comparison to it has more merit. Petaev et al. (1994) modeled a system with a Divnoe composition while varying the oxygen fugacity and found that at an fO_2 of IW-1.8, the olivine composition and metal content matched that of Divnoe. This fO_2 is intermediate between that which we calculated for Tafassasset (~IW-1) and that calculated by Benedix et al. (2005) for the winonaites and silicate-rich IAB irons (~IW-2.5 to IW-3).

We conclude that Tafassasset is a primitive achondrite similar to the brachinite-like LEW 88763 and Divnoe ungrouped primitive achondrites because of the following: (1) a recrystallized texture with abundant 120° triple junctions, (2) absence of relict chondrules or textures linking it to a specific chondrite group, (3) more "oxidized" olivine and pyroxene composition similar to Divnoe, LEW 88763 and the brachinites, (4) a slightly depleted refractory lithophile and siderophile element composition, (5) evidence of generation and partial removal of both a Fe,Ni–FeS and basaltic partial melt, and (6) fO_2 formation conditions similar to Divnoe. We find these reasons make the noble gas inventory measured by Patzer et al. (2003) consistent with other primitive achondrites.

4.2. Composition of precursor rock

Although Tafassasset is a primitive achondrite, the question still remains: could it be a partially melted meteorite that originated on the CR chondrite parent body as we currently know it? The answer to this question must take into consideration the oxidation state of Tafassasset. As we discussed in Gardner-Vandy et al. (2009), the oxidation state of Tafassasset could be caused by two different scenarios: (1) partial melting of an oxidized chondritic parent body whose oxidation state was established in a high fO_2 region of the solar nebula (material like the CK or R chondrites), or (2) partial melting of a reduced chondritic parent body that accreted ice or hydrated silicates, with the principal oxidizing agent being water released by dehydration of the hydrous phases to increase the fO_2 condition during melting (material like the CR chondrites). The limiting factor for Tafassasset is formation under a calculated fO_2 of ~IW-1. Any formation mechanism must take this into account, as well as the high abundance of metal and the FeO-rich nature of the silicate minerals in Tafassasset.

The CR chondrites are composed mostly of chondrules (~48–63 vol.%) and a fine-grained matrix (~30–50 vol.%) that contains anhydrous and hydrous silicates, Ca-carbonates, sulfides, and magnetite (Weisberg et al., 1993; Kallemeyn et al., 1994; Krot et al., 2002). The chondrule population on the CR chondrite parent body is mostly (~99%) type-I chondrules that contain olivine between Fa_0 and Fa_{10} (Weisberg et al., 1993; Kallemeyn et al., 1994). While type-II chondrules that contain olivine $>Fa_{15}$ are present in CR chondrites, their abundance is, at most, 3.5 vol.% of the chondrule population (Schrader et al., 2011).

When considering a CR chondrite as the precursor material to Tafassasset, a problem arises when considering the bulk Fe content of the various parts of CR chondrites compared to the bulk Fe content of the three chips of Tafassasset analyzed here. Mean Fe content for the CR chondrites is 24 wt.% Fe (Kallemeyn et al., 1994), and even though CR matrix contains more FeO in hydrated silicates and magnetite, analyzes of matrix regions show that the matrix is a maximum of 28 wt.% Fe (Weisberg et al., 1993; Zolensky et al., 1993; Abreu and Brearley 2010). The three Tafassasset chips analyzed here have between 23 and 40 wt.% Fe. In order to maintain mass balance during oxidation of a CR chondrite precursor (with Fe,Ni-metal, Fe-sulfide, FeO-poor silicates, and Fe- and FeO-bearing matrix) to generate a Tafassasset-like product (with Fe,Ni-metal, Fe-sulfide, and FeO-rich silicates), the reaction would require the introduction of excess Fe into the system. This would be the case even if the Tafassasset precursor was composed entirely of CR chondrite matrix. This is an unlikely scenario given the current knowledge of the CR chondrite parent body.

The only way to get Tafassasset from a CR chondrite is to have a parent body made entirely of type-II chondrules and matrix, and this is also extremely unrealistic, given the low abundance of type-II chondrules in the CR chondrule population. Likewise, Connolly and Huss (2010) found that oxygen isotopic compositions of type-II chondrules in CR2 chondrites span a wide range, many plotting in 3-isotope space above the terrestrial fractionation line (near the ordinary chondrite field). Thus, a partially melted meteorite comprised of type-II chondrules would likely plot away from the CR chondrite trend. Because Tafassasset plots near the CR trend, we know this is not the case.

Finally, despite having oxygen isotopic compositions along the CR chondrite trend and higher metal abundance than the CRs, the CH and CB chondrites (also members of the CR clan) have silicates too FeO-poor to account for the formation of Tafassasset (Weisberg et al., 2001). Therefore, we exclude them as the possible precursor material of Tafassasset as well.

As a result of these considerations, we propose that Tafassasset formed from an FeO-rich chondritic precursor that is currently unsampled in the meteorite collection. This parent body likely incompletely melted and cooled without reaching isotopic homogeneity (as seen in Tafassasset's oxygen isotopic composition) in a region of the nebula with oxygen isotope composition similar to the CR chondrites.

5. CONCLUSIONS

Tafassasset is an olivine-dominated meteorite with a high metal abundance given the FeO-rich content of its silicates. Despite an oxygen isotope composition near the CR chondrite trend, we classify it as a primitive achondrite similar to LEW 88763 and Divnoe based upon its achondritic

texture, FeO-rich silicate composition, and a depleted refractory lithophile and siderophile composition. We rule out a relationship with the CR chondrite parent body as we currently know it. It is likely Tafassasset originated on a body that partially melted, never reached isotopic equilibrium, and came from the same oxygen isotopic reservoir as the CR chondrites. Tafassasset is an extraordinary meteorite and is the first metal-rich primitive achondrite with an oxidized silicate mineralogy. Its presence in the meteorite collection further emphasizes the complexity of planetesimals that existed in the early solar system.

ACKNOWLEDGEMENTS

We thank Ken Domanik for help with EMPA and use of the IQmaterials™ program, Yulia Goreva for help with ICP-MS technique, Mark Ghiorso for supplying the supplemental MELTS calculator, and both Harold C. Connolly, Jr. and Devin Schrader for many useful discussions about CR chondrites. We also think the Southwest Meteorite Laboratory and the Museum National d'Histoire Naturelle in Paris, France for donating large chips of Tafassasset and loaning us many thin sections for analysis. This work was funded by NASA Grants NNX09AQ88H and NNX10AH50G to D.S.L. and the University of Arizona/Alfred P. Sloan Foundation Indigenous Graduate Partnership Fellowship to K.G.G.V.

REFERENCES

Abreu N. M. and Brearley A. J. (2010) Early solar system processes recorded in the matrices of two highly pristine CR3 carbonaceous chondrites, MET 00426 and QUE 99177. *Geochim. Cosmochim. Acta* **74**, 1146–1171.

Anderson D. J., Lindsley D. H. and Davidson P. M. (1993) QUILF: a PASCAL program to assess equilibria among Fe–Mg–Ti oxides, pyroxenes, olivine, and quartz. *Comput. Geosci.* **19**, 1333–1350. Available from: www.geosciences.stonybrook.edu/people/faculty/lindsley/lindsley.html.

Benedix G. K., Lauretta D. S. and McCoy T. J. (2005) Thermodynamic constraints on the formation conditions of winonaites and silicate-bearing IAB irons. *Geochim. Cosmochim. Acta* **69**, 5123–5131.

Bourot-Denise M., Zanda B. and Javoy M. (2002) Tafassasset: an equilibrated CR chondrite. *Lunar Planet. Sci. XXXIII*. Lunar Planet. Inst., Houston. #1611 (abstr.).

Buchwald V. F. (1975). , 904 p.

Bunch T. E., Irving A. J., Larson T. E., Longstaffe F. J., Rumble D. and Wittke J. H. (2005) "Primitive" and igneous achondrites related to the large and differentiated CR parent body. *Lunar Planet. Sci. XXXVI*. Lunar Planet. Inst., Houston. #2308 (abstr.).

Clayton R. N. and Mayeda T. K. (1996) Oxygen isotope studies of achondrites. *Geochim. Cosmochim. Acta* **60**, 1999–2017.

Clayton R. N. and Mayeda T. K. (1999) Oxygen isotope studies of carbonaceous chondrites. *Geochim. Cosmochim. Acta* **63**, 2089–2104.

Clayton R. N., Onuma N., Grossman L. and Mayeda T. K. (1977) Distribution of the presolar component in Allende and other carbonaceous chondrites. *Earth Planet. Sci. Lett.* **34**, 209–224.

Connolly, Jr., H. C. and Huss G. R. (2010) Compositional evolution of the protoplanetary disk: oxygen isotopes of type-II chondrules from CR2 chondrites. *Geochim. Cosmochim. Acta* **74**, 2473–2483.

Gardner K. G., Lauretta D. S. and Killgore M. (2007) Petrology of ungrouped achondrites RBT 04239 and Tafassasset: a comparison to Divnoe and the brachinites. *Lunar Planet. Sci. XXXVIII*. Lunar Planet. Inst., Houston. #1338 (abstr.).

Gardner-Vandy K. G., Lauretta D. S., Killgore M., Franchi I. A. and Greenwood R. C. (2008) Tafassasset: the saga continues. *Lunar Planet. Sci. XXXIX*. Lunar Planet. Inst., Houston. #2307 (abstr.).

Gardner-Vandy K. G., McCoy T. J., and Lauretta D. S. (2009) Formation conditions of the FeO-rich primitive achondrites (abstract). *Lunar Planet. Sci. XL*. Lunar Planet. Inst., Houston. #2520 (abstr.).

Gardner-Vandy K. G., Hill D. H., Lauretta D. S., Goreva Y. S., Domanik K. J., Greenwood R. C., Franchi I. A. and Killgore M. (2011) Petrology and geochemistry of the Northwest Africa 3368 Eucrite. *Meteorit. Planet. Sci.* **46**, 1052–1070.

Goldstein J. I. and Michael J. R. (2006) The formation of plessite in meteoritic metal. *Meteorit. Planet. Sci.* **41**, 553–570.

Göpel C., Birck J. L. and Manhès G. (2009) U/Pb and Cr isotope study of the Tafassasset meteorite. *Meteorit. Planet. Sci.* **44**, A5267 (abstr.).

Greenwood R. C., Franchi I. A., Gibson J. M. and Benedix G. K. (2007) Oxygen isotope variation of the primitive achondrites. *Lunar Planet. Sci. XXXVIII*. Lunar Planet. Inst., Houston. #1338 (abstr.).

Hirschmann M. M. (1991) Thermodynamics of multicomponent olivines and the solution properties of (Ni, Mg, Fe)2SiO4 and (Ca, Mg, Fe)2SiO4 olivines. *Am. Mineral.* **76**, 1232–1248.

Imai N., Terashima S., Itoh S. and Ando A. (1995) 1994 compilation of analytical data for minor and trace elements in seventeen GSJ geochemical reference samples, "Igneous rock series". *Geostand. Newsl.* **19**, 135–213.

Irving A. J., Kuehner S. M. and Rumble D. (2005) Brachinite NWA 3151 and (?)Brachinite NWA 595. *Meteorit. Planet. Sci.* **40**, A5213 (abstr.).

Kallemeyn G. W., Rubin A. E. and Wasson J. T. (1994) The compositional classification of chondrites: VI. The CR carbonaceous chondrite group. *Geochim. Cosmochim. Acta* **58**, 2873–2888.

Kimura M., Grossman J. N. and Weisberg M. K. (2008) Fe–Ni metal in primitive chondrites: indicators of classification and metamorphic conditions for ordinary and CO chondrites. *Meteorit. Planet. Sci.* **43**, 1161–1177.

Koblitz J. (2005) *MetBase: Meteorite Data Retrieval Software, version 7.2 for Windows*. Brenman, Germany.

Krot A. N., Meibom A., Weisberg M. K. and Keil K. (2002) The CR chondrite clan: implications for early solar system processes. *Meteoritic. Planet. Sci.* **37**, 1451–1490.

Kushiro I. and Mysen B. O. (1979) Melting experiments on a Yamato chondrite. *Proc. 4th Symp. Antarctic Met., Mem. Natl. Inst. Polar Res.* **15**, 165–170.

McCoy T. J., Keil K., Clayton R. N., Mayeda T. K., Bogard D. D., Garrison D. H., Huss G. R., Hutcheon I. D. and Wieler R. (1996) A petrologic, chemical, and isotopic study of Monument Draw and comparison with other acapulcoites: evidence for formation by incipient partial melting. *Geochim. Cosmochim. Acta* **60**, 2681–2708.

McCoy T. J., Keil K., Clayton R. N., Mayeda T. K., Bogard D. D., Garrison D. H. and Wieler R. (1997) A petrologic and isotopic study of lodranites: evidence for early formation as partial melt residues from heterogeneous precursors. *Geochim. Cosmochim. Acta* **61**, 623–637.

Miller M. F., Franchi I. A., Sexton A. S. and Pillinger C. T. (1999) High precision $\Delta^{17}O$ measurements of oxygen from silicates and other oxides: methods and applications. *Rapid Commun. Mass Spectrom.* **13**, 1211–1217.

Miller M. F. (2002) Isotopic fractionation and the quantification of ^{17}O anomalies in the oxygen three-isotope system: an appraisal and geochemical significance. *Geochim. Cosmochim. Acta* **66**, 1881–1889.

Mittlefehldt D. W., McCoy T.J., Goodrich C. A. and Kracher A. (1998) Non-chondritic meteorites from asteroidal bodies. In *Planetary Materials* (ed. J. J. Papike). *Rev. Mineral.*, **36**. Mineralogical Society of America, Washington DC. pp. 4–1–4–495.

Mittlefehldt D. W., Bogard D. D., Berkley J. L. and Garrison D. H. (2003) Brachinites: igneous rocks from a differentiated asteroid. *Meteorit. Planet. Sci.* **38**, 1601–1625.

Morse S. A. (1994) *Basalts and Phase Diagrams*. Corrected and reprinted by Krieger Publishing Company, Melbourne, Florida, 493 pp.

Nehru C. E., Prinz M., Delaney J. S., Dreibus G., Palme H., Spettel B. and Wänke H. (1983) Brachina: a new type of meteorite, not a chassignite. *Proc. 14th Lunar Planet. Sci. Conf.: J. Geophys. Res* **88**(suppl.), B237–B244.

Nehru C. E., Weisberg M. K., Boesenberg J. S. and Kilgore M. (2003) Tafassasset: a metal-rich primitive achondrite with affinities to brachinites. *Lunar Planet. Sci. XXXIV*. Lunar Planet. Inst., Houston. #1370 (abstr.).

Patzer A., Schultz L. and Franke L. (2003) New noble gas data of primitive and differentiated achondrites including Northwest Africa 011 and Tafassasset. *Meteorit. Planet. Sci.* **38**, 1485–1497.

Petaev M. I., Barsukova L. D., Lipschutz M. E., Wang M.-S., Ariskin A. A., Clayton R. N. and Mayeda T. K. (1994) The Divnoe meteorite: petrology, chemistry, oxygen isotopes and origin. *Meteorit. Planet. Sci.* **29**, 182–199.

Rubin A. E. (2007) Petrogenesis of acapulcoites and lodranites: a shock-melting model. *Geochim. Cosmochim. Acta* **71**, 2383–2401.

Russell S. S., Zipfel J., Grossman J. N. and Grady M. M. (2002) The Meteoritical bulletin, No. 86, 2002 July. *Meteorit. Planet. Sci.* **37**, A157–A184.

Sack R. O. and Ghiorso M. S. (1989) Importance of considerations of mixing properties in establishing an internally consistent thermodynamic database: thermochemistry of minerals in the system Mg_2SiO_4–Fe_2SiO_4–SiO_2. *Contrib. Mineral. Petrol.* **102**, 41–68.

Sack R. O. and Ghiorso M. S. (1991a) Chromite as a petrogenetic indicator. In *Oxide Minerals: Petrologic and Magnetic Significance* (ed. D. H. Lindsley), *Rev. Mineral.* **25**. Mineralogical Society of America, Washington DC. pp. 323–353.

Sack R. O. and Ghiorso M. S. (1991b) Chromian spinels as petrogenetic indicators: thermodynamics and petrological applications. *Am. Mineral.* **76**, 827–847.

Schrader D. L., Franchi I. A., Connolly, Jr., H. C., Greenwood R. C., Lauretta D. S. and Gibson J. M. (2011) The formation and alteration of the Renazzo-like carbonaceous chondrites I: implications of bulk-oxygen isotopic composition. *Geochim. Cosmochim. Acta* **75**, 308–325.

Swindle T. D., Kring D. A., Burkland M. K., Hill D. H. and Boynton W. V. (1998) Noble gases, bulk chemistry, and petrography of olivine-rich achondrites Eagles Nest and Lewis Cliff 88763: comparison to brachinites. *Meteorit. Planetary Sci.* **33**, 31–48.

Takahashi E. (1983) Melting of a Yamato L3 chondrite (Y-74191) up to 30 kbar. *Proc. 8th Symp. Antarctic Met. Mem. Natl. Inst. Polar Res.* **30**, 168–180.

Warren P. H. and Kallemeyn G. W. (1989) Allan Hills 84025: the second brachinite, far more differentiated than Brachina, and an ultramafic achondritc clast from L chondrite Yamato 75097. *Proc. 19th Lunar Planet Sci. Conf.*, 475–486.

Weisberg M. K., Prinz M., Clayton R. N. and Mayeda T. K. (1993) The CR (Renazzo-type) carbonaceous chondrite group and its implications. *Geochim. Cosmochim. Acta* **57**, 1567–1586.

Weisberg M. K., Prinz M., Clayton R. N., mayeda T. K., Sugiura N., Zashu S. and Ebihara M. (2001) A new metal-rich chondrite grouplet. *Meteorit. Planet. Sci.* **36**, 401–418.

Wlotzka F. (1993) A weathering scale for the ordinary chondrites (abstract). *Meteorit. Planet. Sci.* **28**, A460 (abstr.).

Young E. D. and Russell S. S. (1998) Oxygen reservoirs in the early solar nebula inferred from an Allende CAI. *Science* **282**, 452–455.

Zipfel J., Palme H., Spettel B. and Schönbeck T. (2002) Bulk composition of Tafassasset–Evidence for incipient melting. *Meteorit. Planet. Sci.* **37**, A155 (abstr.).

Zolensky M., Barett R. and Browning L. (1993) Mineralogy and composition of matrix and chondrule rims in carbonaceous chondrites. *Geochim. Cosmochim. Acta* **57**, 3123–3148.

Associate editor: Hiroko Nagahara